New Nanoparticle Formation under UV Impact on Acetaldehyde Vapor in Nitrogen and Air Flow

Galina I. Skubnevskaya,[†] **Sergei N. Dubtsov,**[*,†] **Evgeni N. Dultsev,**[†] **Galina G. Dultseva,**[†] **and Wing Tsang**[‡]

Institute of Chemical Kinetics and Combustion of Siberian Branch of RAS, Novosibirsk, 630090, Russia, and National Institute of Standards and Technology, Gaithersburg, Maryland

Received: February 11, 2004; In Final Form: June 7, 2004

This paper deals with the study of the kinetics of photolysis and photonucleation of acetaldehyde (AA) vapor in air and in nitrogen along with physical and chemical characteristics of the formed aerosol particles. Free radicals accompanying photonucleation were identified using the electron spin resonance spin-trapping technique. Numerical modeling of the photonucleation kinetics of AA, based on experimental results, was carried out. Rate of generation of primary products, leading to the nanoparticles, and the aerosol yield were evaluated. Chemical mechanism of stages leading to photonucleation in this system was proposed.

1. Introduction

Chemical processes providing gas-to-particle conversion in the atmosphere play a key role in regulating cloud condensation nuclei, changing the actinic flux of UV radiation, and affecting the climate.[1] The formation of aerosol particles under UV photolysis of gaseous substances is one of the ways to generate organic particulate matter in the atmosphere and an efficient removal pathway for volatile impurities. Over the past decade, the formation and growth of the nanometer-sized atmospheric aerosol particles have been detected in a number of sites. These observations are summarized and analyzed in the review of Kulmala et al.[2]

Since the pioneering studies of the Los Angeles smog,[3] many attempts have been made to achieve a detailed understanding of the photochemically induced nucleation. The knowledge in physical organic chemistry dealing with this process is accumulated in well-known books.[4−6] However, the photochemical transformation of organics into aerosols is poorly understood yet. It is in striking contrast to the gas-phase conversion processes.

This paper deals with nucleation kinetics and specific properties of ultrafine particles induced by aldehyde vapor photodecomposition in the air and nitrogen. Acetaldehyde (AA) represents a typical combustion-generated pollutant from the diesel engines and power plant plumes. This aldehyde is highly reactive in the atmosphere; it is the major precursor of peroxyacetylnitrate in polluted air. The ability of AA to serve as photoinitiator and precursor of ultrafine organic particles is an actual and open question. As it follows from classic thermodynamic considerations, pure AA does not form aerosol particles.[4] However, quite an opposite conclusion can be made keeping in mind the ability of AA to undergo oligomerization. There is great practical importance in developing thorough quantitative investigations of the pathways of AA conversion, including aerosol formation, to compose realistic models of

atmospheric chemistry and create the atmospheric pollutant control strategies.

Experimental Section

The kinetics of UV photolysis of AA vapor was studied with the experimental set-up consisting of a reagent mixture preparation unit and the laminar flow cylindrical quartz reactor (inside diameter, 22 mm; length, 200 mm; Re < 70), illuminated with unfocused full-spectrum light of a Hg low-pressure lamp (DRT-240). In some runs, the short-wavelength spectral region (<320 nm) was cut off by optical glass filters (UFS-2, ZhS-3). Relative intensity I/I_o of irradiation was varied from 10^{-2} to 10^{-6} by changing the distance between the lamp and the reactor. Irradiation time t was varied from 0.02 to 30 s by changing the irradiated volume of the reactor. The reactor was "preconditioned" by UV irradiation of the reagent mixture flow for several hours before measurements to improve the reproducibility. Carrier gases were nitrogen (99.995%), a mixture of nitrogen with oxygen (99.995%) 4:1, and air purified by passing through a HEPA filter and a column with 4 Å molecular sieves. The AA vapor was obtained by bubbling the flow of carrier gas through liquid CH_3CHO (Fluka, assay > 99.5%) which was distilled ($T_{boil} = 20.5−21.5$ °C, $n^{17}_d = 1.3316$) immediately before measurements and thermostated at 250 ± 2 K. AA concentration in carrier gas flow was varied within $(0.15−7.0) \times 10^{17}$ molecule/cm^3, as monitored by measuring the UV absorption at 290 nm with a HP 8354 spectrophotometer, and by means of high-performance liquid chromatography (HPLC) using a preliminary reaction of CH_3CHO with 2,4-dinitrophenylhydrazine to yield the hydrazone.[7] In some experiments, water and hydrogen peroxide vapor were added into the reaction mixture. Twice-distilled water and H_2O_2 (16%) of "chemically pure" reagent grade were used for these purposes. Water vapor concentration in the reaction flow was varied from 0.5 to 2.8 $\times 10^{17}$ molecule/cm^3 and controlled with a flow hygrometer.

To measure the concentration of UV-generated aerosol particles, the Novosibirsk Automated Diffusion Battery (NADB) was used.[8] It consists of a turbulent mixing condensational enlarger, 8-stage screen-type diffusion battery (DB), photoelectric particle counter, and microprocessor-based controller for

---

* To whom correspondence may be addressed. E-mail: dubtsov@ns.kinetics.nsc.ru. Phone: +7-383-2-33-15-19. Fax: +7-383-2-34-23-50.
† Institute of Chemical Kinetics and Combustion of Siberian Branch of RAS.
‡ National Institute of Standards and Technology.

data acquisition and transfer to a PC.[9,10] A multiple solution averaging algorithm[17] was used to convert the DB data into particle-size distribution. This NADB was tested during an international workshop on intercomparison of different types of condensation particle counters.[8] It was shown that the NADB can measure particle concentration N_a in the range of 10^1-10^7 cm^{-3} and mean diameter in the range of 3–200 nm. The absolute accuracy of N_a measurement is ±10%. For a given fixed set of intensity or time of irradiation and reagent concentration, reproducibility of N_a values in different experimental runs is ±40%. A set of 8 measurements was averaged to obtain each point on the $N(I,t)$ plot.

To study temperature dependence of photolysis and photonucleation, the reactor was equipped with a heater; the temperature in the reactor was maintained during experiments within the range 290–450 K with an accuracy of ±2 K, as controlled with a copper–constantan thermocouple.

A collection of aerosol samples (∼0.5 mg) for chemical analysis was carried out using a flow quartz reactor of larger volume, higher concentration of AA (up to 2×10^{18} molecules/cm^3), and higher intensity of UV irradiation. Aerosol samples were collected at the exit of this reactor for 0.5–4 h using glass fiber, paper, and Teflon filters, as well as a 4-stage low-pressure impactor with Teflon substrates. Two identical blank filters and substrates were used in each run along with the working filter to avoid misinterpretation. One of the blanks was placed at the outlet of the reactor with the flow of gas mixture without irradiation (to take into account of the processes in the dark), another was kept idle. The aerosol samples collected on the working filters were extracted using solvents: benzene, ethanol, or water. Blank filters were treated similarly. Melting points, solubility, redox parameters, and UV absorption of the aerosol samples were determined, with blanks as references. The physicochemical properties of aerosol collected with the filters of all types were similar to each other, while impactor-collected samples gave quite different characteristics, for example, a higher melting point. It can be assumed that some low-boiling fractions are lost in impactor-collected samples. Glass fiber filters were chosen for our studies as the most reliable and efficient ones among the tested filters.

Chemical composition of gaseous and aerosol products of AA photolysis was examined with GC and HPLC as described elsewhere[7] and by means of UV (in ethanol), IR (in tablets with KBr, and in chloroform), and NMR (in deuterated chloroform) spectroscopy.

Photochemically generated short-lived free radicals were studied as follows. The concentrating glass tubes placed at the outlet of the photochemical quartz flow reactor were filled with crushed quartz and impregnated with an aqueous solution of a spin trap (0.1 M, 0.2 mL). The flow of reaction mixture coming out of the reactor passed through this tube for 10–30 min. The spin trap reacted with short-lived radicals to form spin adducts. These adducts were dissolved in a small amount of water (ca. 0.5 mL), which was poured into a standard quartz electron spin resonance (ESR) cell. The ESR spectra of spin adducts were recorded with a BRUKER ER-200 D-SRC spectrometer as described in detail elsewhere.[11] Since the known spin traps phenyl-*tert*-butyl nitrone (PBN) and dimethylpyrroline oxide (DMPO) were insufficiently stable in our system, we used new nitrone spin traps: pentamethylimidazoline *N*-oxide **I** (**PMIO**) and conjugated dihydropyrazine dioxides with different substituents **II** and **III**. They were chosen among 42 aldonitrone compounds synthesized in cooperation with the Novosibirsk Institute of Organic Chemistry. All of these
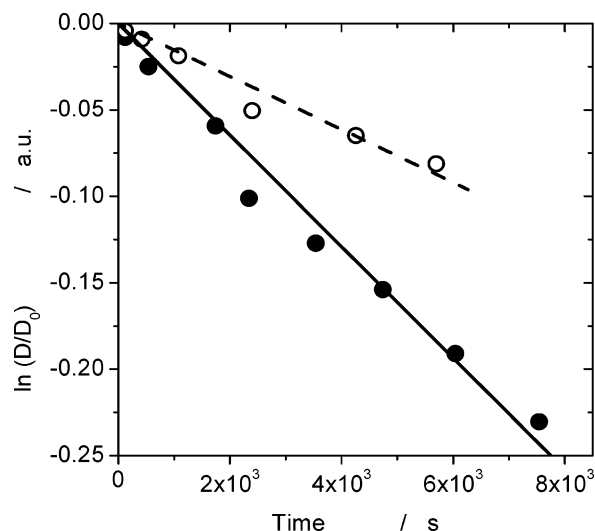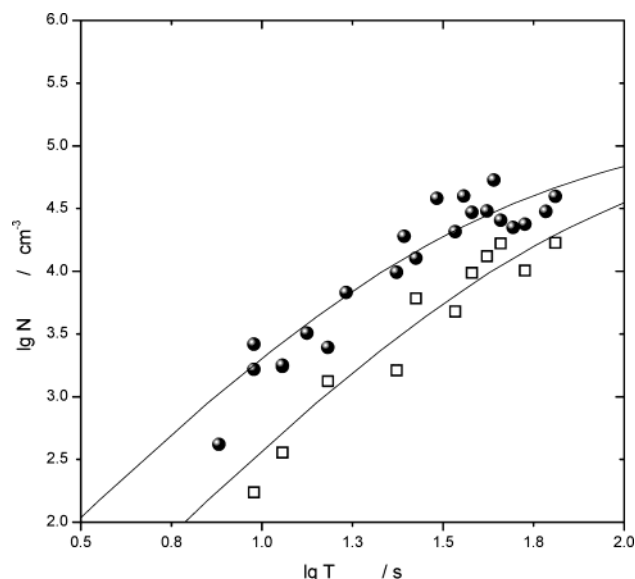

Figure 1. Photolysis kinetics of AA in nitrogen and in synthetic air (80% N_2 + 20% O_2) at room temperature. [CH_3CHO] = (3.45 ± 0.50) × 10^{17} molecule/cm^3. [H_2O] = ca. 0.5 × 10^{17} molecule/cm^3. Experimental data: ●, 80% N_2 + 20% O_2; ○, pure N_2. Lines indicate a linear fit.

spin traps were preliminarily tested in solution in model systems with the generation of various short-lived free radicals: OH, HO_2, CH_3, HCO, C_6H_5, etc. The hyperfine splitting constants of various spin adducts were tabulated as a reference for identifying spin adducts formed in the gaseous systems under investigation.

I   **II**   **III**
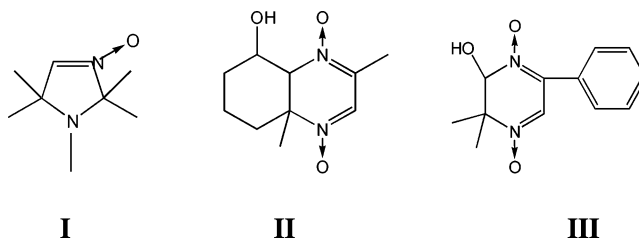
Results and Discussions

1. Kinetics of AA Photolysis in Nitrogen and in Air. During the UV photolysis at room temperature, AA consumption follows the first-order kinetics in the inert gas and in air as it is shown in Figure 1. The effective photolysis rate constants, determined from the initial slope of the kinetic curves, were equal to (1.53 ± 0.17) × 10^{-5} s^{-1} in nitrogen and (3.23 ± 0.17) × 10^{-5} s^{-1} in a N_2–O_2 (4:1) mixture. Dark adsorption on the walls of the cell was taken into account when calculating these values. Under UV irradiation of AA vapor in nitrogen flow at ca. 85 °C, both photolysis and thermolysis take place. Measurements showed that the rate of photochemical decomposition exceeds the rate of thermal decomposition by a factor of 2. In heating alone and in the joint action of heating and irradiation, the kinetics of AA decomposition exhibits two regions: (1) within irradiation time interval from 0 to ca. 400–450 s, a rapid decay of CH_3CHO concentration occurs ($k_{decomp1} = 1.4 \times 10^{-3}$ s^{-1} for thermolysis and 3.3 × 10^{-3} s^{-1} for photolysis), and (2) for time longer than 450 s, a slower decay is observed ($k_{decomp2} = 1.1 \times 10^{-4}$ s^{-1} for thermal decomposition and 2.4 × 10^{-4} s^{-1} for photolysis). A novel fact was discovered: the formation of an intermediate gas-phase product at the initial stage of photolysis at elevated temperature. It absorbs light in the spectral region 190–210 nm and decomposes under further irradiation. The UV spectroscopic study showed that the absorption

New Nanoparticle Formation Impact on Acetaldehyde

J. Phys. Chem. B, Vol. 108, No. 31, 2004 **11395**

Figure 2. Kinetics of AA photochemically induced aerosol formation in nitrogen and in synthetic air (20% O_2 + 80% N_2) at room temperature. [CH_3CHO] = $(3.45 \pm 0.50) \times 10^{17}$ molecule/cm^3. [H_2O] = ca. 0.5×10^{17} molecule/cm^3. Experimental data: □, 80% N_2 + 20% O_2; ●, pure N_2. Lines indicate a numerical simulation.

spectrum of this product is similar to the UV spectra of the AA trimer and tetramer, which we isolated from the aged liquid AA sample and dissolved in hexane. The NMR and HPLC examinations confirmed the structure of these species as AA oligomers. Thus, assumption can be made that photolysis stimulates the AA oligomerization in the gas phase.

2. Kinetics of Photochemical Aerosol Formation (Photonucleation) of AA. Photonucleation may be observed upon UV irradiation of AA vapor in N_2 or air flow only with a wavelength shorter than 320 nm. The dark stages are of no importance. We discovered that only freshly distilled AA forms aerosol. Typical kinetic curves of aerosol formation during UV exposure of AA in nitrogen or air flow are shown in Figure 2, presenting the dependences of concentration of formed photoaerosols (N_a) on irradiation time at a constant intensity of irradiation. When irradiation intensity is varied with irradiation time kept constant, only some changes in the positions of the curves are observed. Carrier gas (nitrogen, air) affects the kinetics of AA photonucleation. The aerosol formation rate is about 2−6 times higher in nitrogen than in air. Note that the rate of AA photolysis in nitrogen is ca. two times lower than that observed in air. Thus, as shown in Figures 1 and 2, foreign gas affects AA photonucleation and photolysis in the opposite directions. The combination of AA irradiation and heating of the reactor above 60−70 °C increases the rate of aerosol formation in nitrogen, compared with irradiation alone.

A single-mode size distribution is observed in photochemically generated aerosol particles. The mean diameter of aerosols increases with irradiation time from 6 to 10 nm both in N_2 and in air. For equal irradiation time t, the size of particles formed in N_2 and in air is about the same.

The influence of water vapor on the AA aerosol formation kinetics was checked. Water was found to increase the rate of aerosol formation both in air and in nitrogen. As for the AA photolysis kinetics, the observed photolysis rate constant k_{phot} (s^{-1}) decreases slightly with an increase in water concentration and may be expressed as follows: $k_{phot} = k_0 - (1.38 \pm 0.37) \times 10^{-22} \times [H_2O]$, for nitrogen, and $k_{phot} = k_0 - (1.22 \pm 0.20) \times 10^{-22} \times [H_2O]$, for synthetic air. Water concentration is

expressed in molecule/cm^3. k_0 is the photolysis rate constant, extrapolated to zero water vapor concentration.

3. Numerical Modeling of Aerosol Formation Kinetics. To evaluate the rate of the monomer formation $F(t)$, numerical modeling of aerosol formation kinetics has been performed. The Smoluchowski equation was solved for free-molecular collisions of monomers and clusters, similar to those described by Rao and McMurry.[12] An effective algorithm for solving the coagulation equation has been reported earlier by Dubtsov et al.[9,10,13] In the present study, this model was modified to account for the influence of t_1 (time gap between the end of irradiation and the moment of particles detection) and diffusion losses of monomer and clusters on the walls of the reactor and pipelines. Similarly to Rao and McMurry,[12] the main approximations of this model are the following:

(a) The rate of monomer formation $F(t)$ is constant with time;

(b) All collisions of clusters and monomers are effective, i.e., result in the formation of new clusters; and

(c) The evaporation of monomers from clusters is negligible.

Under these conditions, the dynamics of the particle concentration is described by the following equations

$$dN_1/dt = -N_1 \sum_{i=1}^{\infty} \beta_{1i} N_i + F(t) \qquad (1)$$

$$dN_k/dt = {}^1\!/_2 \sum_{i+j=k} \beta_{ij} N_i N_j - N_k \sum_{i=1}^{\infty} \beta_{ki} N_i \qquad (2)$$

where $F(t) = F =$ constant at $t \le t_0$, $F(t) = 0$ at $t_0 \le t \le t_0 + t_1$ (no monomer formation during t_1), β_{ij} is the collision constant for clusters, consisting of i and j monomers, N_k is the concentration of clusters, consisting of k monomers, t_0 is the irradiation time, and t_1 is the retention time. According to Rao and McMurry,[12] we consider substitution of variables

$$N_i = k_n n_i \qquad t = k_\tau \tau \qquad \text{where} \quad k_n = (F/\beta_{11})^{1/2}$$
$$k_\tau = (1/F\beta_{11})^{1/2} \quad (3)$$

Then, eqs 1 and 2 reduce to the form

$$dn_1/d\tau = \tilde{F} - n_1 \sum_{i=1}^{\infty} K_{1i} n_i \qquad (4)$$

$$dn_k/d\tau = {}^1\!/_2 \sum_{i+j=k} K_{ij} n_i n_j - n_k \sum_{i=1}^{\infty} K_{ki} n_k \qquad (5)$$

where $\tilde{F}(\tau) = 1$ when $\tau \le \tilde{\tau} \le \tilde{\tau} + \tilde{\tau}$ and $\tilde{F}(\tau) = 0$ when $\tilde{\tau}_0 \le \tilde{\tau} \le \tilde{\tau}_0 + \tilde{\tau}_1$, where $\tilde{\tau}_0 = \tau_0/k_\tau$, $\tilde{\tau}_1 = \tau_1/k_\tau$, $\tilde{\gamma}_k = \gamma_k/k_\tau$, and $K_{ij} = \beta_{ij}/\beta_{11}$. For the free-molecular collisions regime, we have[12]

$$K_{ij} = {}^1\!/_4 \sqrt{2} (i^{1/3} + j^{1/3})^2 (1/i + 1/j)^{1/2} \qquad (6)$$

The Cauchy problem (eqs 4−5) is solved by a sectional algorithm, suggested by Koutzenogii et al.[14] For approximation of the aerosol size distribution, 50-point and 80-cubic finite elements are used. The monomer formation rate value was calculated by a nonlinear least-squares fitting of the calculated curves with experimental data by a technique similar to that described by Dubtsov et al.[9,10]

Foreign gas affects the rate of monomer formation (F). Thus, in N_2, $F = 1.48 \times 10^7$ cm^{-3} s^{-1}, which is more than in the N_2 + O_2 mixture (4:1) $F = 0.742 \times 10^7$ cm^{-3} s^{-1}, when water concentration is less than 5.0×10^{17} molecule/cm^3. The aerosol
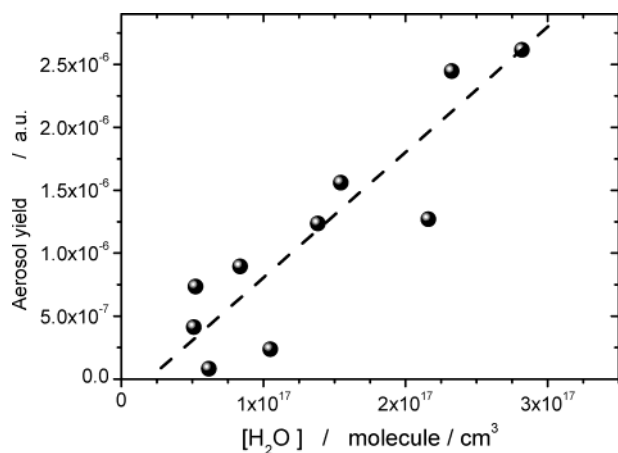
Figure 3. Aerosol yield of AA photonucleation in $N_2 + O_2$ mixture vs water concentration. CH_3CHO concentration range: from 1.5×10^{17} to 3.5×10^{17} molecule/cm^3. ●, experimental values; line, linear fit.

TABLE 1: ESR Parameters of Spin Adducts Formed under CH_3CHO Vapor Flow Photolysis

spin trap	hsc in nitrogen			hsc in air		
	a_N, mT	a_H, mT	$\tau_{1/2}$, min	a_N, mT	a_H, mT	$\tau_{1/2}$, min
I: room temp	1.46	2.92	27	1.70	1.97	12
II: room temp and 125°C	1.46	2.31	15	1.43	1.42	4
III: room temp and 125°C	1.49	2.45	19	1.44	1.61	15

yield was calculated as a ratio of the monomer formation rate to the AA photolysis rate

$$1.0 \times 10^{-6} - \Theta = F/k_{photo}[CH_3CHO] \qquad (7)$$

The experimentally measured photolysis rate in photonucleation experiments was equal to 8.93×10^{12} and 6.66×10^{12} cm^{-3} s^{-1} for air and nitrogen, respectively. So, the aerosol yield equals to 8.01×10^{-7} in air and 2.2×10^{-6} in nitrogen. An increase in water concentration leads to an increase in the F value. Figure 3 shows the dependence of the aerosol yield vs water concentration for AA photolysis in the $N_2 + O_2$ mixture (4:1).

The addition of hydrogen peroxide vapor (in mixture with water vapor) caused a 2-fold decrease in aerosol yield in comparison with water vapor alone. We believe this decrease is due to the increased rate of reaction route leading to gas-phase products via the interaction of AA itself and intermediates with the added OH radical.

4. Identification of Active Intermediates of the Process.
AA is known to undergo the radical and molecular decomposition as the primary stages of UV photolysis. We detected the

**TABLE 2. Gas-Phase Products Formed of AA Photolysis in N_2 and in Air Flow at 20 °C (in % reacted AA)**

N_2	air
diacetyl (2)	
acetone (0.3)	acetone (5)
glyoxal (0.8)	glyoxal (2.4)
formaldehyde (up to 12)	formaldehyde (0.04)
acyclic aldehydes C_6 and C_8	
AA trimer, tetramer (see Figure 4)	
	methyl glyoxal (0.5)
	acids (total 22.4):
	formic, acetic, peracetic

spin adducts of short-lived free radicals in AA vapor photolyzed both in air and in nitrogen using the spin trapping ESR technique. Hyperfine splitting constants (hsc) in the ESR spectra of the spin adducts are listed in Table 1.

One can see that different spin adducts were formed in nitrogen and in air. The hyperfine splitting constants of the spin adduct with **I** obtained in N_2 ($a_N = 1.46$ mT, $a_H = 2.92$ mT) allowed us to attribute this signal to the CH_3 adduct, on the basis of the previous examination in model system with CH_3 generated by a standard procedure. The ESR signal obtained in air ($a_N = 1.70$ mT, $a_H = 1.97$ mT) belongs to the CH_3O- PMIO spin adduct.

Unfortunately, a spin trap **I** was unsuitable at elevated temperature. Because of this, nitrones with better thermal stability **II** and **III** were chosen for experiments at elevated temperature (125 °C). In the dark at $T = 125$ °C and [CH_3CHO] = 130 Torr in nitrogen flow (0.5 l/min) without irradiation, no ESR signals were detected, which means that no thermolysis-generated free radicals were present in the reaction mixture. Under photolysis, spin adducts of **II** and **III** with CH_3^* were detected both at room temperature and at 125 °C, though in the latter case the concentration of spin adducts was about 40% smaller than at room temperature. In air flow, spin adducts of **II** and **III** with RO*-type radicals were detected, in particular CH_3O^*, both at room and at elevated temperature; in the latter case, the concentration of spin adducts was higher by a factor of 1.5−1.7. We did not observe spin adducts of OH or HO_2 either at room temperature or at 125 °C. Since these spin traps were efficient in trapping OH and HO_2 in model systems, we may assume that these radicals are consumed via some mechanisms in the system with AA vapor, similar to those described by Tomas et al.[15] It should be noted that we detected the spin adducts of OH with **I**, **II**, and **III** when hydrogen peroxide was specially added to the reaction mixture to be photolyzed.

5. Gas and Aerosol Products of AA Photolysis. The major gas-phase products of AA photolysis are CH_4 and CO.[16] We
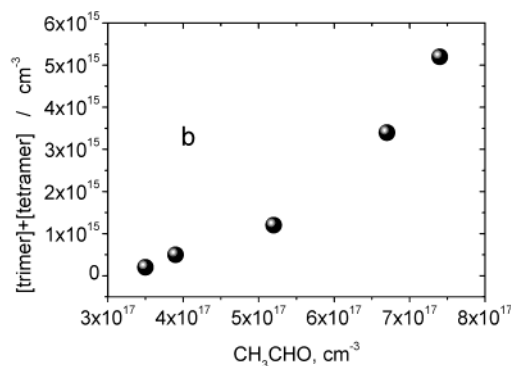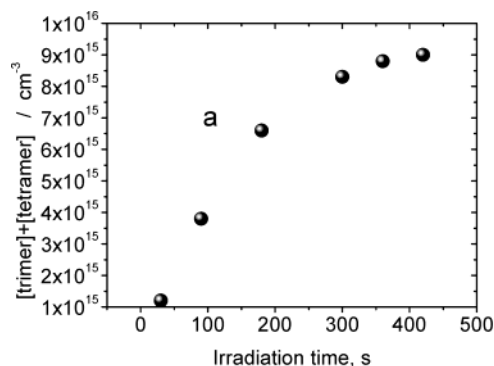
Figure 4. (a) Total concentration (cm^{-3}) of AA trimer and tetramer in nitrogen vs irradiation time for initial CH_3CHO concentration 5.2×10^{17} cm^{-3}. (b) Total concentration of AA trimer and tetramer vs CH_3CHO concentration for 30 s irradiation time.

investigated minor gaseous products of AA photolysis. The composition of gas products depended on the carrier gas (Table 2).

In N_2, the trimer concentration was about 3 times higher than that of tetramer, as determined by HPLC. Total concentration of these oligomers was found to depend on AA concentration and irradiation time (parts a and b of Figure 4).

In air as the carrier gas, large amounts of acetic and peracetic acid were formed during the AA photolysis. The concentrations of acids depended on irradiation time. We assume that these acids promote nucleation in AA vapor in the presence of oxidizing additive (oxygen), keeping in mind that organic acids are known initiators of AA polymerization in liquid.
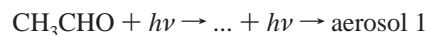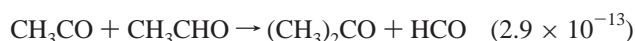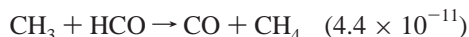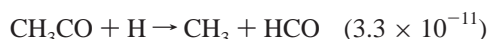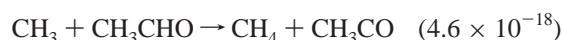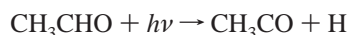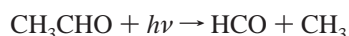
At increased temperature (90−120 °C), a dark reaction was detected in which gaseous diacetyl was formed (about 0.7%); it was never detected in the dark at room temperature. Both for N_2 and for air, higher-temperature gaseous products were qualitatively the same as those at room temperature, except for peracetic acid, which was not detected in the gas phase at 120 °C (detection limit: ∼0.2%).

The aerosol products obtained in AA vapor in nitrogen flow contained carbonyl groups and exhibited strong reducing properties; under storage in weakly acidic medium, it released AA trimers and tetramers, which we detected by means of HPLC. Elemental analysis revealed that the H:C:O atomic ratio of aerosol product (in N_2) was similar to that of the initial AA (4:2:1). This fact suggests that trimers and tetramers $(CH_3CHO)_n$ ($n = 3$ and 4) are the initial species for AA photonucleation in nitrogen. At increased temperature, the composition of the aerosol products was the same; however, the aerosol yield somewhat increased in comparison to that observed at room temperature.
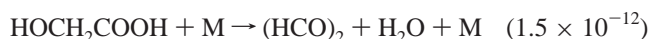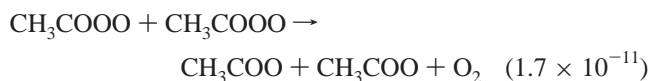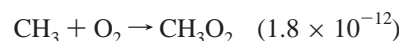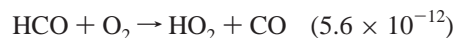
Aerosol products formed under AA photolysis in air exhibited strong oxidative properties and contained no carbonyl groups. The H:C:O atomic ratio of the aerosol product was 3.6:2.7:1.8, which is quite different from the starting one. By means of qualitative chemical analysis, we discovered that the aerosol formed in AA + air is composed of oxygenated species including peroxy O−O bonds.

Thus, different final products in the gas phase and aerosols were detected under AA photolysis in nitrogen and in air. The results of chemical identification give us grounds to suppose that different free radicals (CH_3 in N_2 and CH_3O in air) lead by different reaction routes to chemically unequal aerosol products in inert gas and in the air.

The supposed chemical mechanism of AA phototransformation into gas and aerosol products was numerically modeled using the NIST Chemical Kinetics Database, version 2Q98. AA phototransformations in nitrogen can be schematically represented by the reaction sequence (first-order rate constants, s; second-order rate constants, cm^3/s)

$$CH_3CHO + h\nu \rightarrow HCO + CH_3$$

$$CH_3CHO + h\nu \rightarrow CH_3CO + H$$

$$CH_3 + CH_3CHO \rightarrow CH_4 + CH_3CO \quad (4.6 \times 10^{-18})$$

$$CH_3CO + H \rightarrow CH_3 + HCO \quad (3.3 \times 10^{-11})$$

$$CH_3 + CH_3CO \rightarrow (CH_3)_2CO \quad (7.0 \times 10^{-11})$$

$$CH_3CO + HCO \rightarrow CH_3COCHO \quad (3.0 \times 10^{-11})$$

$$CH_3 + HCO \rightarrow CO + CH_4 \quad (4.4 \times 10^{-11})$$

$$CH_3CO + CH_3CHO \rightarrow (CH_3)_2CO + HCO \quad (2.9 \times 10^{-13})$$

$$HCO + HCO \rightarrow (HCO)_2 \quad (5.0 \times 10^{-11})$$

$$CH_3CO + CH_3CO \rightarrow CH_3COCOCH_3 \quad (1.8 \times 10^{-11})$$

$$CH_3CHO + h\nu \rightarrow ... + h\nu \rightarrow \text{aerosol 1}$$

In the presence of oxygen, the following reactions also become essential

$$HCO + O_2 \rightarrow HO_2 + CO \quad (5.6 \times 10^{-12})$$

$$HCO + O_2 \rightarrow HC(O)O_2 \quad (1.1 \times 10^{-11})$$

$$CH_3 + O_2 \rightarrow CH_3O_2 \quad (1.8 \times 10^{-12})$$

$$CH_3O_2 + CH_3O_2 \rightarrow 2CH_3O + O_2 \quad (3.7 \times 10^{-13})$$

$$HO_2 + CH_3O_2 \rightarrow CH_3OOH + O_2 \quad (5.6 \times 10^{-12})$$

$$CH_3CO + O_2 \rightarrow CH_3COOO \quad (5.0 \times 10^{-12})$$

$$CH_3COOO + HO_2 \rightarrow CH_3COOOH + O_2 \quad (1.4 \times 10^{-11})$$

$$CH_3COOO + HO_2 \rightarrow CH_3COOH + O_3 \quad (1.1 \times 10^{-11})$$

$$CH_3COOO + CH_3O_2 \rightarrow$$
$$CH_3COO + CH_3O + O_2 \quad (8.8 \times 10^{-12})$$

$$CH_3COOO + CH_3COOO \rightarrow$$
$$CH_3COO + CH_3COO + O_2 \quad (1.7 \times 10^{-11})$$

$$CH_3COOO + CH_3COOO \rightarrow$$
$$CH_3OCOCOOCH_3 + O_2 \quad (1.5 \times 10^{-10})$$

$$CH_3CHO + O_2 \rightarrow HOCH_2COOH \quad (4.2 \times 10^{-18})$$

$$HOCH_2COOH + M \rightarrow (HCO)_2 + H_2O + M \quad (1.5 \times 10^{-12})$$

$$CH_3CHO + h\nu \rightarrow ... + CH_3COOOH + h\nu \rightarrow \text{aerosol 2}$$

These reaction sequences illustrate the possible routes to minor products that were detected in the gas-phase AA photolysis, e.g., acetone, glyoxal, methyl glyoxal, and diacetyl. In addition, they show the possible fate of the HO_2 radical reacting to form organic acids.

The role of the OH radical may be reduced to directing the reaction route to the gaseous products starting with the reaction

$$CH_3CHO + OH = CH_3CO + H_2O$$
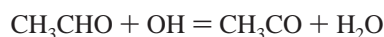
which causes a decrease in the yield of particulate matter.

Conclusions

The photodecomposition of AA vapor involving minor stages generating aerosol has been studied in detail. Special attention was paid to the regularities of aerosol particles formation, the dependence of aerosol concentration on irradiation time and intensity, as well as on the nature of carrier gas and additives (water). Oxygen increases the rate of AA photolysis and

decreases the rate of aerosol formation (F), while water vapor decreases photolysis rate and increases F. To understand this effect, we studied the intermediate, gas, and aerosol products of photochemical transformations of AA depending on the nature of carrier gas. It was shown that CH_3 and HCO free radicals are formed in the primary stage of AA photolysis and initiate photonucleation in nitrogen resulting in the formation of the product with reductive properties. In the presence of oxygen, these radicals are transformed into HO_2, CH_3O_2, and CH_3O (the latter was detected by the spin-trapping technique) and lead to the formation of the aerosol products with strong oxidative properties. Modeling of photonucleation, combined with fitting to the experimental results, allowed us to calculate aerosol generation rate, which was higher in N_2 than in air. The formation of the discovered intermediates, gas, and aerosol products was described using the databases on the kinetics of atmospheric reactions.

References and Notes

(1) *The chemistry of the atmosphere: its impact on global change: a chemistry for the 21st century monograph*; Calvert, J. G., Ed.; Blackwell Science: New York, 1994; p 394.

(2) Kulmala, M.; Vehkamäki, H.; Petäjä, T.; Dal Maso, M.; Lauri, A.; Kerminen, V.-M.; Birmili, W.; McMurry, P. H. *J. Aerosol Sci.* **2004**, *35*, 143−176.

(3) Haagen-Smit, A. J.; Bradley, C. E.; Fox M. M. *Ind. Eng. Chem.* **1953**, *45*, 2086−2094.

(4) Seinfeld, J. H.; Pandis, S. N. *Atmospheric Chemistry and Physics: From Air Pollution to Climate Change*; J. Wiley: New York, 1997.

(5) Finlayson-Pitts, B. J.; Pitts, J. N. *Atmospheric Chemistry: Fundamentals and Experimental Techniques*; John Wiley: New York, 1986.

(6) Isidorov, V. A. *Organic Chemistry of the Atmosphere*; Khimizdat: St. Petersburg, 2001.

(7) Skubnevskaya, G. I.; Dultseva, G. G. *J. Ecol. Chem.* **1994**, *3*, 29−34.

(8) Reschl, G. P.; Ankilov, A. I.; Baklanov, A. M.; Mavliev, R. A.; Eremenko, S. I.; Majerowicz. *J. Aerosol Sci.* **1991**, *22*, S325 −S326.

(9) Dubtsov, S. N.; Dultsev, E. N.; Dultseva, G. G.; Skubnevskaya, G. I. *Chem. Phys. Rep.* **2000**, *18*, 1609−1614.

(10) Dubtsov, S. N.; Levykin, A. I.; Sabelfeld, K. K. *J. Aerosol Sci.* **2000**, *31*, 509−518.

(11) Dultseva, G. G.; Skubnevskaya, G. I.; Volodarsky, L. V.; Tikhonov, A. Ya.; Mazhukin, D. G. *J. Phys. Chem.* **1996**, *100*, 17523−17527.

(12) Rao, N. P.; McMurry, P. H. *Aerosol Sci. Technol.* **1992**, *11*, 120−137.

(13) Dubtsov, S. N.; Koutzenogii, K. P.; Levykin, A. I.; Skubnevskaya, G. I. *J. Aerosol Sci.* **1995**, *26*, 705−716.

(14) Koutzenogii, K. P.; Levykin, A. I.; Sabelfeld, K. K. *J. Aerosol Sci.* **1996**, *27*, 679−688.

(15) Tomas, A.; Villenave, E.; Lesclaux, R. *J. Phys. Chem.* **2001**, *105*, 3505−3514.

(16) Calvert, J. G.; Pitts, J. N., Jr. *Photochemistry* Wiley: NY, 1966.

(17) Eremenko, S. E.; Ankilov, A. N. *J. Aerosol. Sci.* **1995**, *26*, S5749−S5750.